IEEE Access
Multidisciplinary | Rapid Review | Open Access Journal

Received August 20, 2020, accepted October 9, 2020, date of publication October 20, 2020, date of current version October 30, 2020.

Digital Object Identifier 10.1109/ACCESS.2020.3032535

Design and Parameter Optimization of Disc Type Cutting Device for Castor Stem

JUNMING HOU, JINGBO BAI, ENCHAO YAO, AND HONGJIE ZHU
School of Engineering, Shenyang Agricultural University, Shenyang 100866, China
Corresponding author: Junming Hou (junming_hou@163.com)

This work was supported by the China National Natural Science Foundation project under Project 51457312.

ABSTRACT To increase the cutting efficiency for castor stem, the castor harvester cutting device was developed. The structure of the disc cutting device was designed. Cutting blade angle, sufficient working and minor cutting edge lengths were determined, which were 20°, 73 mm and 19.8 mm, respectively. The finite element model of disc cutter for castor stem was established. The incision volume was selected as the cutting performance evaluation index. The cutting process of the cutter was simulated. The results show that the cutting performance of the trapezoidal cutter is preferable to that of the rectangular and the curved cutters. When cutting blade cuts the stem, the volume of the incision decreases first and then increases, and the size of the incision increases with the increase of cutting edge angle. When the blade angle is 10°, the cutter has the ideal cutting quality. Considering the blade angle, the slip angle, and the angle of the cutter head as factors, the virtual test of the cutter was made with the incision volume as the index. The response surface analysis was used to obtain the cutter structure parameters when the incision volume was the least. The result for the blade, slip and cutter head inclination angles are 14.06°, 19.93°, and 10.54°, respectively. The cutting efficiency evaluation index (one-time cutting) was established to optimize the cutter running parameters. The results show that when the cutter moving speed was 1.011 m/s and the cutter rotation speed was 282.0 r/min, the maximum cutting efficiency is 2.25 castor stems/s.

INDEX TERMS Castor stem, cutting, design, finite element, optimized design.

I. INTRODUCTION

Mechanized harvesting of castor is efficient for increasing the yield of castor. The cutting device of the castor harvest machine is a critical component that directly determines the cutting effect of the castor stem.

Several studies on agricultural material cutting devices have been conducted. Rovira-Más *et al.* [1] designed a vegetation-cutting device that automatically sets the speed to adjust to the motor speed by a sensor module mounted on the output shaft. Tian *et al.* [2] used the bionic principle to design a cutting tooth straw device, which can effectively reduce the cutting resistance and power consumption. Kroes and Harris [3] developed a kinematic model of sugar cane harvester, which describes the base cutter kinematics of the sugar cane harvester. Jia *et al.* [4] applied the bionic principle to design a saw blade for corn stalk cutting and used Matlab software to obtain an outer margin profile from the stereo-microscope photograph of the serrated incisors. Mathanker *et al.* [5] studied the effects of oblique blade angle and cutting speed on cutting energy for cane stems. Gan *et al.* [6] studied the impact of three cutting blade designs on energy consumption during mowing-conditioning of miscanthus giganteus, and compared the energy requirements of three blades. Halim *et al.* [7] investigated the sharpness of onion cutting knife using an improvised digital microscope. Schmidtthe *et al.* [8] investigated buzz saw blade cutting forces for cutting frozen wood depending on tool geometries. Li *et al.* [9] used the finite element method to complete a simulation model of corn stubble cutting verified by the field tests. Meng *et al.* [10] applied an explicit kinetic simulation method and experimental study of circular saw blade cutting system for the small mulberry cutting machine. They used ANSYS/LS-DYNA software to establish three-dimensional finite element models of the bulletin saw blade cutting system.

Li *et al.* [11], [12] designed an air-blown wheat cutting testing platform, which can effectively reduce the loss of wheat grains at the cutting platform compared with the traditional grain-wheel cutting platform. Tang *et al.* [13] used Adams

The associate editor coordinating the review of this manuscript and approving it for publication was Aneel Rahim.

software to analyze the cutting process of cannabis stalk, then obtained the changing rule of cutting force with time in the cutting process. Cao *et al.* [14] used ANSYS/LS-DYNA to study the influence of different structural parameters and motion parameters of the safflower picking device on the posture of safflower during the picking process. Chen *et al.* [15] built a simplified model of a sugarcane cutting tool, and studied the influence of parameters on the dynamic characteristics of the system. By establishing the motion equation of the planetary wheel drive mechanism, Ran *et al.* [16] analyzed the motion structure parameters of the cutter, which is satisfied by the driving mechanism. Gao *et al.* [17] proposed a study on a 2D optimization simulation of complex five-hole cutting blasting under different lateral pressure coefficients of 400 m and 800 m with ANSYS/LS-DYNA software, and analyzed the evolution rules of blasting cracks and lateral pressure coefficients. Lou *et al.* [18] used ANSYS/LS-DYNA software for numerical simulation to provide a logical theoretical solution to determine center hole and cutting parameters.

However, the design for the castor stem cutter was not studied. To the best of our knowledge, the relationship of the cutter structure parameters and cutting effect is not considered. In this study, the self-designed castor stem cutting device was considered as the research object. The influence of different cutter parameters on the cutting performance was investigated using the finite element method. We performed virtual test, and a set of optimal cuts was determined by response surface analysis. The Adams software was applied to analyze the cutter model and establish the cutting performance evaluation index of the cutter. The results can provide a theoretical basis for the development of castor harvest machine.

II. CUTTING DEVICE DESIGN

A. OVERALL STRUCTURAL DESIGN

Depending on the physical and mechanical characteristics of the castor stem, the disc cutting device was designed. The cutting tool is mainly composed of cutter plate, blade, bearing end cover, cutter shaft, fixed sleeve, bearing, shaft end ring and bevel gear. The cutting device is located directly below the elastic toothed roller, then the whole structure is attached to the frame through a fixing sleeve. A bearing part is embedded inside the sleeve; the cutter shaft passes through the sleeve. One end of the cutter shaft cooperates with the bevel gear, through which power is communicated to the cutter shaft. The other bottom is attached to the cutter head through the spline, and the shaft end retains the ring. Since the disc cutter rotates at high speed, a considerable impact force is generated when contacting the stem; thus, the cutter is easily damaged. Therefore, the connection method can provide the cutter head with torque to ensure power transmission stability, as shown in Fig. 1.

B. CUTTING BLADE EDGE DETERMINATION

The size of the cutting edge angle directly determines the sharpness of the cutter. When the cutter cuts into the

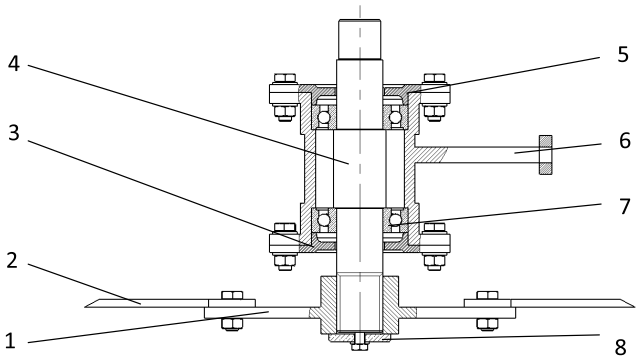

FIGURE 1. Overall structure of cutting device. 1.Cutter plate 2.Blade 3.Lower bearing end cap 4.Cutter shaft 5.Upper bearing end cap 6.Fixed sleeve 7. Bearing 8. Shaft end ring.

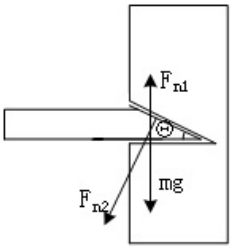

FIGURE 2. Castor stem cutting force diagram.

stem, a composite force relationship occurs between them. Fig. 2 shows the force diagram when the cutter uniformly cuts into the stem.

According to the force analysis:

$$F_{n1} = mg + F_{n2}\cos\theta \tag{1}$$

Then:

$$F_{n2} = \frac{F_{n1} - mg}{cos\theta} \tag{2}$$

where, m——Quality of cutter

F_{n1}——Supporting pressure on lower the scalpel

F_{n2}——Positive pressure on the scalpel

θ——Cutter angle

According to Equation (2), the positive pressure of the steam against the blade surface increases with the blade angle, that is, when θ increases, the cutting force required to cut the stem increases. When designing the cutting edge angle, the inclination should be minimized to enable the cutting blade to cut the stem easily. However, the small cutting edge angle will reduce the overall rigidity of the cutter, reducing the service life of the cutting tool. Therefore, the initial cutting blade angle was 20°.

C. DETERMINE THE EFFECTIVE WORKING LENGTH OF THE CUTTER

In the process of cutting the stem, the combination of different working parameters can cause the cutter to miss cutting or re-cutting. Missing cuts can cause the stems to be cut off smoothly, increasing the rate of crop loss. Re-cutting can

increase the power consumption of the whole machine. The maximum advance distance of the cutter is the maximum distance(S_{max}). When determining the working length of the cutter, the working period is generally obtained as:

$$L = S_{max} + \Delta L \tag{3}$$

where L——Cutter working length, (mm)
S_{max}——Cutter maximum distance, (mm)
ΔL——Working direction wear amount, (mm), According to the mechanical properties of castor stem, ΔL is assumed as 10 mm.

When the center point of the top edge of the cutter passes through the center line of the cutter, the distance covered by the cutter is S, which is also called the advance distance. S value is:

$$S = \frac{60v_m}{Zn} \tag{4}$$

where S——Cutter distance, mm
v_m——Machine forward speed, choose 1 m/s
Z——Number of cutters, choose 4
n——Rotating speed of cutter, choose 240 r/min

The working length of the cutter is calculated as 72.5mm. To cut the stem with a single cut, the actual working length of the cutter should be slightly longer than the calculated length. Therefore, L was selected as 73 mm in this study.

To ensure reliable installation between the cutter and its head, the length of the cutter mounting part is 30 mm, and the overall width of the cutter is 60 mm.

D. DETERMINE THE CUTTING EDGE LENGTH OF THE CUTTER

Fig. 3 shows the state of the cutter when it is in contact with the castor stem.

From the geometric relationship, we can obtain (5).

$$c = b - 2Ltan\beta \tag{5}$$

where, c——Cutting edge length, (mm)
b——Cutter width, (mm)
L——Cutter effective working length, (mm)
β——Slip angle, choose 15°

We calculated c to be 19.8 mm, and the structure of the cutter is shown in Fig. 4.

III. SIMULATION ANALYSIS OF CUTTING PROCESS

The castor stem cutting device is an essential component of the castor harvesting machine. During the cutting process, the stem generates multiple stress and deformation near the contact area with the cutter, which directly affects the cutting effect. To examine the influence of different factors affecting the cutting process, ANSYS/LS-DYNA was employed to simulate the cutting process of the disc cutter [19]–[21].

A. ESTABLISHING A FINITE ELEMENT MODEL

A 3D model was established to simulate the corresponding model of the cutting device. The castor stem is simplified as

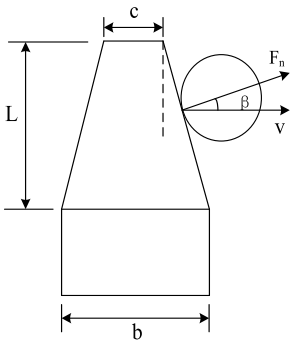

FIGURE 3. Force analysis of Cutter contact stem.

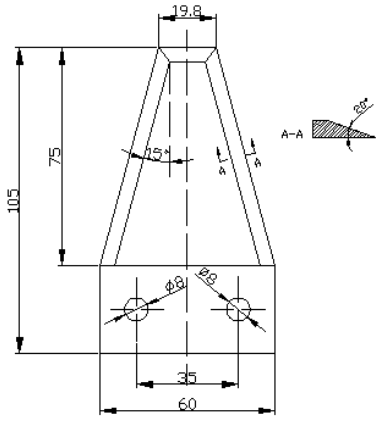

FIGURE 4. Trapezoidal blade.

FIGURE 5. Castor stem model.

follows: (1) The bolt hole of the blade and the cutter head are concentrically matched to remove the bolt connection. (2) Castor stem is a multi-layered grassy shrub, which is mainly composed of xylem, fibrous layer, and pith [22]. Therefore, the castor stem model consists of three layers, and the whole is a hollow cylinder as shown in Fig. 5. The finite element model of the disc cutter cutting the stem is shown in Fig. 6.

B. BOUNDARY CONDITIONS AND MATERIAL PARAMETER SETTINGS

Relevant hypotheses in the finite element analysis process are: (1) The material of each part of the castor stem is simplified as axial isotropic and radial anisotropy. (2) Before loading, the internal stress of the castor stem is zero, and no changes in moisture content and temperature during the simulation. Both the cutter head and the blade are made of structural steel, which has a density of 7850 kg/m^3, Poisson's ratio of 0.3, and an elastic modulus of 2×10^5 MPa. The properties of the castor stem material are shown in Table 1.

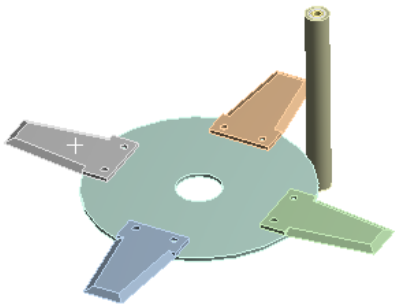

FIGURE 6. Cutting stem finite element model.

TABLE 1. Castor stem material properties.

	Density/ g·cm^{-1}	Elastic Modulus/Mpa	Poisson's ratio
Rod skin	0.18	28	0.314
Fiber layer	0.18	7.375	0.25
Pulp	0.18	4.542	0.192

When the boundary conditions are set, the contact erosion algorithm is established between the cutter and the stem [23]. The static friction coefficient F_S, is 0.3 between the blade and the stem. The dynamic friction coefficient F_D, is 0.2. The rotation speed of the central axis of the cutter head is applied to all nodes on the cutter head and the blade, and the fixed support constraint is applied to one end of the castor stem.

C. SIMULATION ANALYSIS OF CUTTING PROCESS

1) EFFECT OF BLADE SHAPE ON THE CUTTING PROCESS

Fig. 7 presents the variation of stress on the stem when the castor stems are cut by three cutter blades, including a trapezoidal cutter, a curved cutter, and a rectangular cutter. It can be observed that the trapezoidal cutter, the curved cutter, and the square cutter are in contact with the stem at 0.01 s, 0.007s and 0.007 s, respectively.

The stress of the stem increased sharply, which the stress values are 0.66 MPa, 1.76 MPa, and 1.88 MPa, respectively. The contact of the cutter with the stem is important. When the pressure between the cutter and the stem excessively increase, the service life of the blade will be assigned. Depending on the stress value of the contact, the trapezoidal cutter is superior to the other two cutters. When the simulation time is 0.028 s, 0.026 s, and 0.022 s, the stresses of the trapezoidal, curved, and rectangular cutters are at maximum, which are 6.12 Mpa, 6.09 Mpa, and 6.35 Mpa, respectively. The curved cutter is less costly during the cutting process and is superior to the rectangular cutter in use.

Fig. 8 indicates the change of cutting resistance when cutting stems by the three different cutters. It can be observed that the curved knives, trapezoidal knives, and rectangular knives start to produce cutting resistance at a simulation time

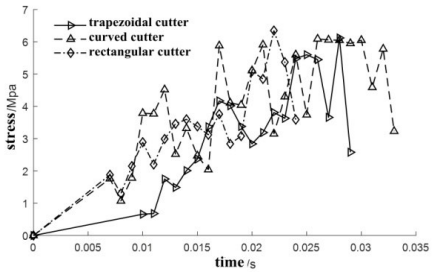

FIGURE 7. Stem equivalent stress.

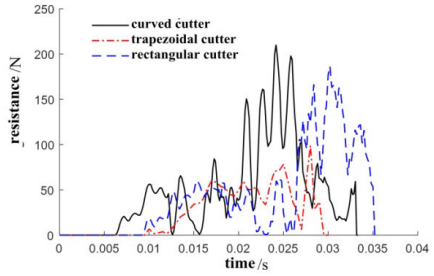

FIGURE 8. Cutter cutting resistance.

of 0.0063 s, 0.01 s, and 0.0092 s, respectively. As the simulation time increases, the cutter continues to cut into the stem, and the cutting resistance continues to grow. The maximum cutting resistance of the curved cutter is 209.885 N, which is higher than that of the rectangular cutter. The curved cutter, trapezoidal cutter, and rectangular cutter are affected by cutting resistance at 0.033 s, 0.030 s, and 0.035 s, respectively. During the cutting stage, the trapezoidal cutter is 0.007 s higher than the curved cutter. Compared with the rectangular cutter, the stem cutting time is advanced by 0.006 s. At the cutting efficiency, the trapezoidal cutter is superior to the other two type cutters. Through comprehensive analysis of cutter life and cutting efficiency, the trapezoidal cutter is ideal for cutting castor stems.

2) INFLUENCE OF THE SLIP ANGLE ON THE CUTTING PROCESS

Fig. 9 shows a stress cloud diagram when the different slicing angle cutters are near the stem. It can be observed that the stem is continuously separated under the action of the blade surface pressing. The stress on the stem is concentrated on the blade face and the lower face. The maximum stress values of the stems were 5.979 Mpa, 6.424 Mpa, 6.086 Mpa, 5.727 Mpa, and 6.053 Mpa at 5°, 10°, 15°, 20°, and 25°, respectively. When the slip angles are 5° and 10°, the quality of the stem cut is rough, indicating that the two small slip angles are severely damaged during the process of cutting the stem. When the cutting angles were 15°, 20°, and 25°, the quality of the stem incision is flush, and the cutting effect of the cutter is visible.

To investigate the cutting performance of different sliding angle cutters, the simulation process is established. Fig. 10 is the incision volume of stem.The stem volume, η, is defined

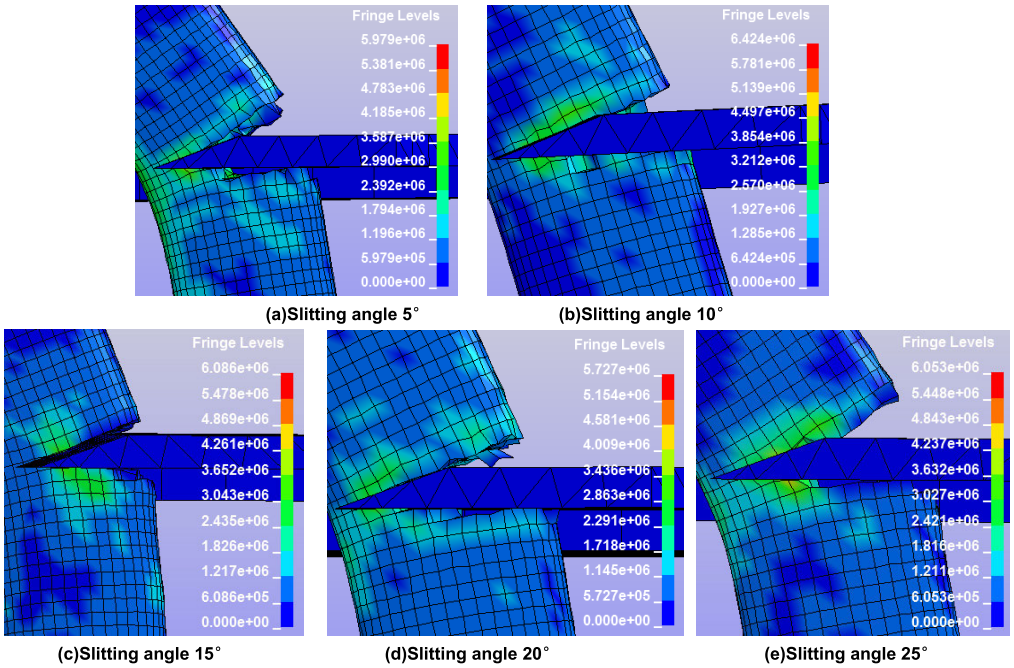

FIGURE 9. Stress cloud diagram of tearing stage of different cutting angle cutters.

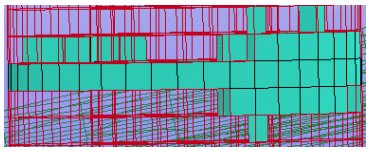

FIGURE 10. Incision volume. Note: When the stem meshes, the sweep method is adopted, and the mesh size is 2 mm. Therefore, when calculating the cutting quality, a single mesh is simplified into a cube with a side length of 2 mm.

as the ratio of the grid failure deletion volume at the slit to the total grid volume of the slit region. As η, becomes small, the more minor the incision in the stem, the cutting quality of the cutter improves. The η calculation method is as follows:

$$\eta = \frac{4vm}{h\pi\left(d^2 - d_1^2\right)} \tag{6}$$

where η——Stem incision volume, (%)
v——Single grid volume, (mm^3)
n——Number of grid deletions
h——Cutting zone height, (mm)
d——Stem diameter, (mm)
d_1——Pulp lumen diameter, (mm)

Fig. 11 shows the quality of the slit corresponding to different slip angles. It can be observed that in the process of cutting, as the slip angle increases, the cutting quality first increases and then decrease when the slip angle is 20°. η is significantly small, and the minimum value is 29.52%. When the slip angle is 5°, η is significantly large, and the maximum value is 38.87%. When the slip angle increases from 5° to 20°, η decreases by 9.7%. When the slip angle increases from 20° to 25°, η is increases by 7.1%. This indicates that the 20° sliding angle cutter has good cutting quality when the stem is touched. That means the incision is flush, and the impact of the cutter is not evident.

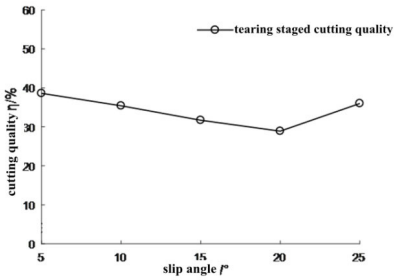

FIGURE 11. Different slip angle cutting quality.

3) INFLUENCE OF CUTTING ANGLE ON THE CUTTING PROCESS

Fig. 12 shows a stress cloud diagram of a different slicing angle cutter when the stem is torn. It can be observed that the stem stress in the tearing stage is mainly distributed on the blade face and the lower face. Under the conditions of 10°, 15°, 20°, 25°, and 30°, the maximum stress value of the stem is 5.915 Mpa, 6.026 Mpa, 6.004 Mpa, 6.105 Mpa, and 5.971 Mpa, respectively. When the blade angle is between 10° and 15°, the friction between the blade surface and the stem is high. The cutter is tightly attached to the internal movement of the stem. The incision has no apparent bearing state. When the blade angle is between 20° and 30°, the cutting action of the cutter is apparent. The stem is forcibly cut; the lower face is ineffective, and the cut is rough.

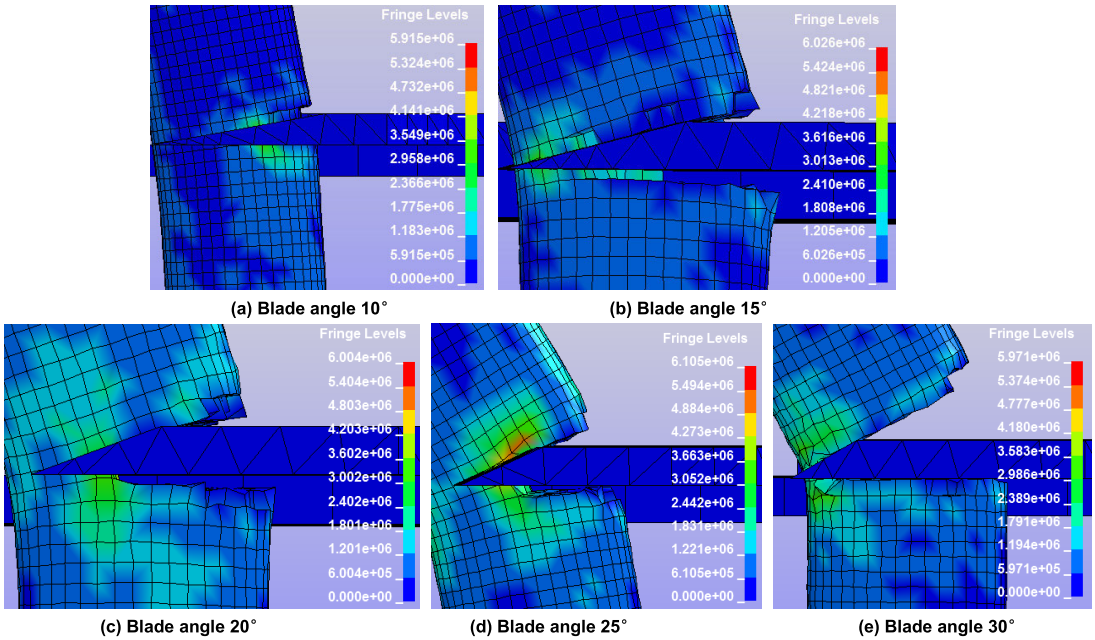

FIGURE 12. Different cloud cutter edge tear stage stress cloud.

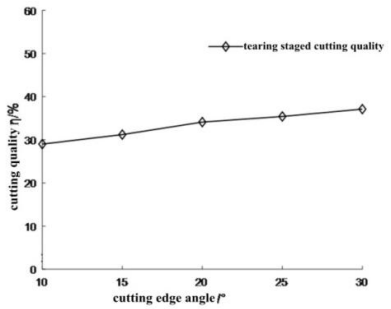

FIGURE 13. Different cutting edge angle cut quality.

Fig.13 shows the quality of the notch corresponding to different blade angles. It can be observed that the cutting quality decreases with the increase of the blade angle during the blade stem phase. When the blade angle is 10°, η is minimum, and the least value is 29.89%. When the blade angle is 30°, η is significantly large, and the maximum value is 35.98%. When the blade angle is increased by 5°, the cutting quality of the cutter is reduced by 2.025% on average. When the blade angle is 10°, the cutter has the ideal cutting quality, and the slit is flush.

IV. CUTTING DEVICE PARAMETER OPTIMIZATION

A. VIRTUAL TEST

To determine the optimal structural parameters of the cutter, the virtual test was carried out. The influence of cutter angle and slip angle was studied. Furthermore, a virtual experiment cutter angle on the cutting force and stem incision volume was conducted. The impact of interactions among factors on the test indicators was analyzed, and a set of optimal cutter parameters was determined.

TABLE 2. Virtual test factor coding table.

Level	Factors		
	Blade angle/°	Slip angle/°	Cutter angle/°
Upper asterisk arm(1.682)	30	25	20
Upper level(1)	25.945	19.932	15.945
Zero level(0)	20	12.5	10
Lower level(-1)	14.055	5.068	4.055
Lower asterisk arm(-1.682)	10	0	0

Note: The slip angle is indirectly characterized by the blade geometry along the blade cutting edge length, i.e. the minor cutting edge length 60 mm corresponds to the slip angle 0°, the minor cutting edge length 46.70 mm corresponds to the slip angle 5.068°, and the minor cutting edge length is 26.75 mm. Corresponding to the slip angle of 12.5°, the minor cutting edge length of 5.61 mm corresponds to the slip angle of 19.932°, and the minor cutting edge length of 0 mm corresponds to the slip angle of 25°.

1) TEST METHOD

TongBi 11 castor stem is selected as the research object, cutter blade angle X_1 (10°-30°), cutter slip angle X_2 (0°-26°) and cutter head inclination angle X_3 (0°-20°) are taken as factors. The stem incision volume when cutting the stem is selected as the experimental evaluation index. The design level of each factor was coded using Design-Export 8.0.6 test design software, as showed in Table 2.

2) ANALYSIS OF RESULTS

The test was carried out by ANSYS/LS-DYNA software using a ternary quadratic general rotation combination

TABLE 3. Simulation test results.

Test number	Factors			Incision volume/ %
	Blade angle/°	Slip angle/°	Cutter angle/°	
1	1	1	1	36.8
2	1	1	-1	36.6
3	1	-1	-1	39.5
4	1	-1	1	35.5
5	-1	1	1	37.1
6	-1	1	-1	33.6
7	-1	-1	-1	39.2
8	-1	-1	1	43.6
9	1.682	0	0	35.8
10	-1.682	0	0	40.2
11	0	1.682	0	38.8
12	0	-1.682	0	41.4
13	0	0	1.682	39.1
14	0	0	-1.682	38.2
15	0	0	0	38.2
16	0	0	0	37.2
17	0	0	0	38.9
18	0	0	0	37.9
19	0	0	0	39.2
20	0	0	0	38.4

method. The test results are shown in Table 3. It can be observed that when the cutter cuts the stem, the stem incision volume is at least 33.6%, and the maximum incision volume is 43.6%.

Regression analysis was carried out between the incision volume of the stem of TongBi 11 and the experimental factors. The ternary quadratic regression equation was obtained as follows:

$$\begin{aligned} Y_2 = {} & 38.34 - 0.92X_1 - 1.32X_2 + 0.41X_3 \\ & + 1.31X_1X_2 - 1.46X_1X_3 + 0.41X_2X_3 \\ & - 0.36X_1^2 + 0.38X_2^2 - 0.13X_3^2 \end{aligned} \tag{7}$$

where Y_2——Stem incision volume, (%)
X_1——Blade angle, (°)
X_2——Slip angle, (°)
X_3——Cutter angle, (°)

To study the influence degree of each test factor on the incision volume of TongBi 11 castor stems, the regression equation (7) was tested for significance and variance analysis (significance level $\alpha = 0.05$). The analysis results are shown in Table 4.

It can be observed from Table 4 that the regression equation of the incision volume of the TongBi 11 castor stem is $P < 0.01$, and the regression model is highly significant. The

TABLE 4. Variance analysis of incision volume simulation test results.

Variation source	Sum of squares	Freedom	Mean squares	*F* Value	*P* Value
Model	74.60	9	8.29	5.47	0.0069**
X_1	11.44	1	11.44	7.55	0.0206*
X_2	23.92	1	23.92	15.78	0.0026**
X_3	2.31	1	2.31	1.52	0.2454
X_1X_2	13.78	1	13.78	9.10	0.0130*
X_1X_3	17.11	1	17.11	11.29	0.0072**
X_2X_3	1.36	1	1.36	0.90	0.3658
X_1^2	1.90	1	1.90	1.25	0.2894
X_2^2	2.08	1	2.08	1.37	0.2688
X_3^2	0.25	1	0.25	0.17	0.6904
Residual	15.15	10	1.52		
Loss of fitting	12.59	5	2.52	4.92	0.0526
Error	2.56	5	0.51		
Total error	89.75	19			

influence on the stem incision volume was significant ($P < 0.01$). The missing term $P = 0.5525 > 0.05$ indicates that the regression equation fits well. It can be used to predict the influence of various factors on the incision volume of TongBi 11 castor stem. Depending on the regression analysis, the order of impact of each factor on the size of stem incision is: Slip angle > Blade angle > Cutter angle. Furthermore, the interaction between the blade angle and the slipping angle has a significant impact on the stem incision volume ($P < 0.05$). The interaction between the blade angle and the cutter angle has a significant effect on the stem incision volume ($P < 0.01$). The simplified regression equation is expressed as:

$$\begin{aligned} Y_2 = {} & 38.34 - 0.92X_1 - 1.32X_2 \\ & + 1.31X_1X_2 - 1.46X_1X_3 \end{aligned} \tag{8}$$

3) RESPONSE SURFACE EFFECTS AND OPTIMIZATION RESULTS OF FACTORS

Fig.14 shows the response surface of the interaction of various factors on the incision volume of TongBi 11 castor stem. It can be observed in Fig.14(a) that when the cutter angle is in the range of 4.05°–10.0°, the volume of the stem cut rapidly increases, and then increases with increase in cutting edge angle. When the cutter angle is in the range of 10°–15.95°, the volume of the stem cut increases with the cutting edge angle. Thus, the interaction between the cutter angle and the blade angle has a significant influence on cutting power consumption ($P < 0.05$). It can be observed from Fig.14(b) that when the blade angle is in the range of 14.06°–20°, the stem

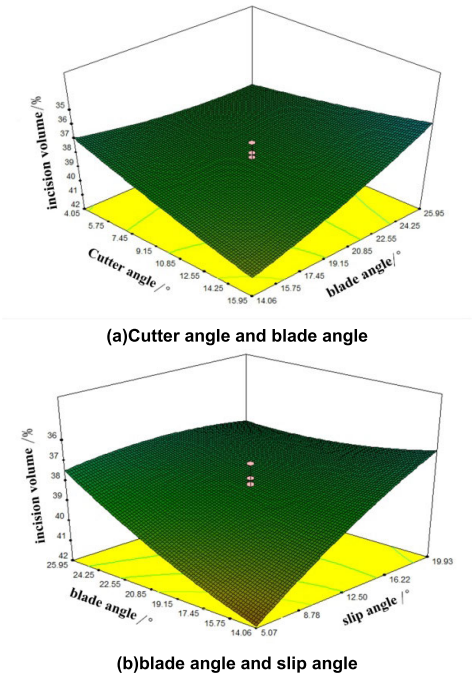

FIGURE 14. Effects of various factors on the incision volume of castor stems in TongBi 11.

incision volume increases with the slip angle. When the blade angle is between 20° and 25.95°, the stem incision volume is significantly large. The rise of the slip angle showed an increase and decrease trend, indicating that the interaction between the blade angle and the slip angle had a significant effect on the stem incision volume ($P < 0.01$).

With the incision volume as the response value, the Design Export software was used to set the target value of the incision volume to a minimum. The minimum predicted value of the incision volume of the castor stem and the parameters of each influencing factor were obtained, that is, the blade angle was 14.06°, and the slip angle was 19.93°. When the angle of the cutter was 10.54°, the incision volume was significantly small, and the minimum value was 36.8%.

B. OPTIMIZATION OF THE MOTION PARAMETERS OF THE CUTTING DEVICE

The combination of cutter speed and forward speed parameters affects the cutting result. In this section, Adams software is used to simulate the cutting process of the cutting blade. By changing the setting of the cutting speed and the forward speed, the influence of different parameter combinations on the cutting efficiency is studied. Therefore, the cutter operating parameters are considered as the design variables, while the cutting efficiency (one cutter cut stem) as the optimization target. The simulation-optimization is carried out to determine a set of optimal operating parameters.

1) INITIAL CONDITIONS AND BOUNDARY CONDITIONS SETTINGS

When the initial conditions are set, it is assumed that the point of cutter blade 1 coincides with the axis of stem 1. The distance is 140 mm from the center of the cutter head. The distance between points n and s in the x-axis direction, the distance between points m and s in the x-axis direction are taken as the optimization target. When the two real-time measured values are small, blades 2 and 3 can cut the stem 2 more significantly, and with high cutting efficiency, as shown in Fig.15.

When the boundary conditions are set, the moving air and the rotating pair are created on the cutter head; a fixed couple connects the castor stem and the ground. The analysis process is performed under the action of the gravity field. The castor stem consists of two sections, and the contact force is added between the two parts. To stop the simulation process, an angle measuring sensor is established at stem 2. When the angle between the two sections of stem 2 is greater than 10°, the simulation is terminated.

2) EFFECT OF SPEED ON CUTTING EFFICIENCY

Considering blade 2 as the research object, Fig. 16 shows the n-s measurement results when stem 2 is cut by blade 2 under different speed conditions. Fig. 17 shows the speed-cutting efficiency curve based on the rational number approximation method.

From Fig.16, as the moving speed of the cutter increases, the time required for the stem to be cut decreases. When the speed is 0.2 m/s, 0.4 m/s, 0.6 m/s, 0.8 m/s, and 1.0 m/s, n-s measurement results when the stem is cut are 6.9457 mm, 4.3126 mm, 23.744 mm, 2.5104 mm, and 2.9134 mm, respectively. The n-s measurement is small and the cutting efficiency is high. From Fig.17, the mathematical model of the cutting speed and n-s measurement results is obtained by (9).

$$y = \frac{0.06341}{x^3 - 1.406x^2 + 0.5090x - 0.06068}$$
$$R^2 = 0.9817 \tag{9}$$

where, y——n-s measurement, mm
x——Cutter moving speed, m/s

3) EFFECT OF SPEED ON CUTTING EFFICIENCY

Fig.18 shows an n-s measurement result when stem 2 is cut by blade 2 under different rotation speed conditions. Fig.19 presents a rotation-cutting efficiency curve fitted based on the Fourier approximation method.

When the rotation speed is 190 r/min, the time required to cut the stem 2 is significantly short. When the rotational speed was 190 r/min, 215 r/min, 240 r/min, 265 r/min, and 290 r/min, the n-s measurement results for cutting were 5.0597 mm, 6.1586 mm, 23.744 mm, 2.9563 mm, and 32.019 mm, respectively. For the cut speed design variable, when the speed is 265 r/min, the n-s measurement is significantly small, and the cutting efficiency is significantly high. From Fig.19, the mathematical model of the cutter speed and n-s measurement results in equation (10):

$$k = 13.01 + 17.69\cos 0.1091n + 0.6997\sin 0.1091n \quad R^2 = 0.9205 \tag{10}$$

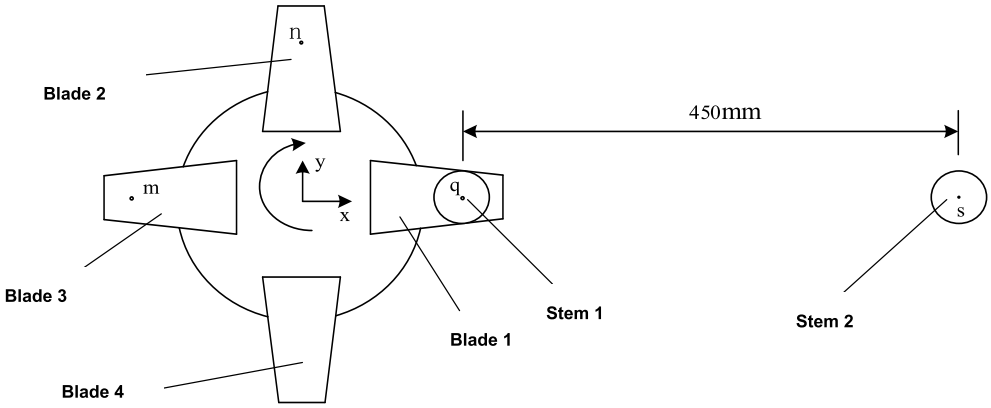

FIGURE 15. Initial condition setting.

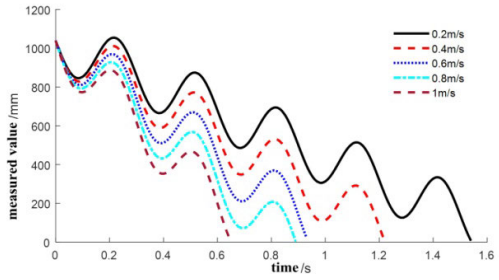

FIGURE 16. n-s measured value-time curve.

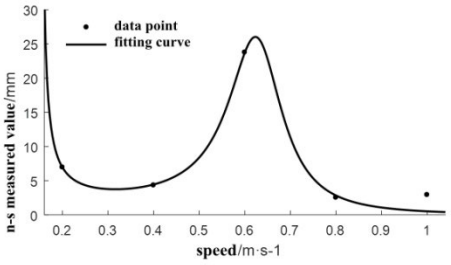

FIGURE 17. n-s measurement - speed curve.

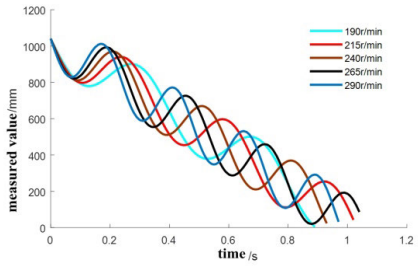

FIGURE 18. n-s measured value-time curve.

where, k——n-s measurement, mm
n——Cutter roation speed, r/min

4) OPTIMIZATION OF OPERATING PARAMETERS

According to the research on the design variable of cutter moving speed and cutter speed, the moving speed is 1 m/s,

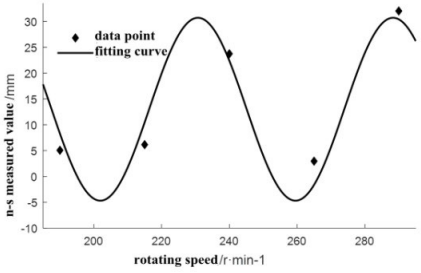

FIGURE 19. n-s measured value-rotating speed curve.

and the cutter rotation speed is 265 r/min, as the design variable center value. The optimization module of Adams is used to optimize the single target parameters. According to the geometric relationship, the n-s and m-s measurements should be less than 2 mm to optimize the termination condition.

Fig.20 shows the results of the first, second, and third optimizations when blade 2 cuts the stem. The minimum value of the first optimization result n-s is 42.3 mm, and the corresponding cutter rotation speed and cutter moving speed are 266.9 r/min and 1.004 m/s, respectively. For the second optimization result, the minimum value of the n-s measurement is 4.0 mm, and the corresponding cutter rotation speed and cutter moving speed are 269.8 r/min and 1.007 m/s, respectively. For the third optimization result, the minimum value of the n-s measurement value is 0.7 mm, and the corresponding cutter speed and cutter advance speed are 269.8 r/min and 1.09 m/s, respectively. Meanwhile, the n-s measurement value is 0.7 mm $<$ 2.0 mm, and thus the optimization is terminated. Therefore, when the cutter roation speed is approximately 269.8 r/min, and the cutter moving speed is approximately 1.009 m/s, the ''one-time cut'' can be achieved, and the cutter cutting efficiency is significantly high.

Fig.21 shows the results of the first and second optimizations when blade 3 cuts the stem. The minimum m-s measurement value of the first optimization result is 4.2 mm, and the corresponding cutter rotation speed and cutter moving speed are 281.8 r/min and 1.007 m/s, respectively. With

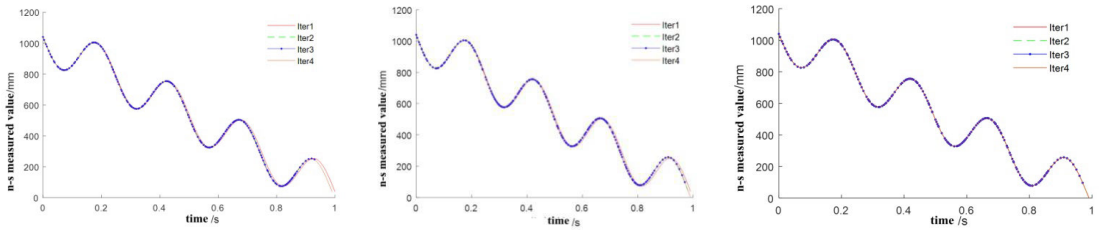

(a)First optimization result (b)Second optimization result (c)Third optimization result

FIGURE 20. Optimization result.

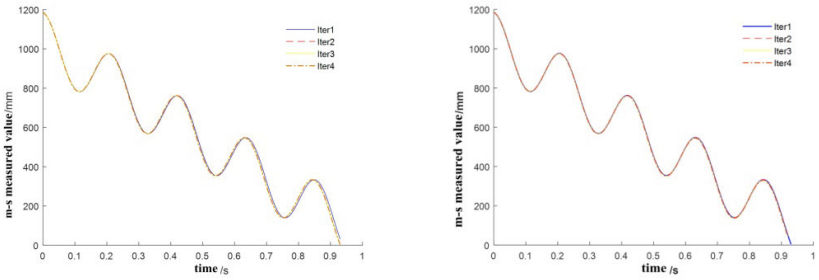

(a)First optimization result (b)Second optimization result

FIGURE 21. Optimization result.

281.8 r/min and 1.007 m/s as initial values, the variable interval is narrowed down for the second optimization. For the second optimization result, the minimum value of the m-s measurement is 1.2 mm, and the corresponding cutter rotation speed and cutter moving speed are 282.0 r/min and 1.011 m/s. Meanwhile, when the m-s measurement value is 1.2 mm $<$ 2.0 mm, the optimization is terminated. Therefore, the rotation speed of the cutter is 282.0 r/min, and the moving speed of the cutter is 1.011 m/s, which can achieve ''one-time cutting''. The cutter has the highest cutting efficiency, which is 2.25 castor stems/s.

V. CONCLUSION

(1) To improve the cutting efficiency, the castor harvester cutting device is considered as the research object, and the overall structure of the cutting device is designed. According to the force analysis of the cutting process, the blade edge angle is determined to be 20.0°, and the cutter works effectively. The cutter working length is 73.0 mm, and the cutter cutting edge length is 19.8 mm.

(2) The influence of different cutter shapes on the cutting process was analyzed. The simulation results show that the trapezoidal cutter is superior to the rectangular cutter. The mesh failure in the incision and the total mesh volume ratio in the incision area are the cutting mass η. The influence of different blade angles and slip angles on the cutting quality is analyzed when the cutter cuts the stem stage along with the slip angle. When the volume is increased, the volume of the incision first decreased and then increased. The change is apparent; the volume of the incision increases with the increase of the blade angle.

(3) Considering the blade angle, the slip angle, and the cutter angle as the factors, the cutting volume of the cutter is used as the index for the virtual test. The test results show that the blade angle has a significant influence on the incision volume,

(4) The slip angle has a significant influence on the incision volume. The interaction between the cutter angle and the blade angle as well as between blade angle and the slipping angle have a significant effect on the incision volume. According to the response surface analysis, the cutter structure parameters were determined, which are blade angle 14.06°, slip angle 19.93°, and cutter head inclination 10.54°. The cutter parameters is obtained based on the rational number approximation and the Fourier approximation methods. The model of optimized parameters was developed. The optimization results show that the highest cutting efficiency is 2.25 castor stems/s when the cutting moving speed is 1.011 m/s, and the cutter rotation speed is 282.0 r/min.

ACKNOWLEDGMENT

The authors would like to thank relevant scholars for their assistance in the literature. They would also like to thank Editage Company for English language editing.

REFERENCES

[1] F. Rovira-Más, Q. Zhang, J. F. Reid, and J. D. Will, ''Machine vision based automated tractor guidance,'' *Int. J. Smart Eng. Syst. Des.*, vol. 5, no. 4, pp. 467–480, Oct. 2003, doi: 10.1080/10255810390445300.

[2] K. P. Tian, X. W. Li, C. Shen, J. C. Huang, J. G. Wang, and Y. Zhou, ''Design and test of cutting blade of cannabis harvester based on longicorn bionic principle,'' *Trans. Chin. Soc. Agricult. Eng.*, vol. 33, no. 5, pp. 56–61, May 2017, doi: 10.11975/j.issn.1002-6819.2017.05.008.

[3] S. Kroes and H. D. Harris, "A kinematic model of the dual basecutter of a sugar cane harvester," *J. Agricult. Eng. Res.*, vol. 62, no. 3, pp. 163–172, Nov. 1995, doi: 10.1006/jaer.1995.1074.
[4] H. L. Jia, C. Y. Li, Z. H. Zhang, and G. Wang, "Design of bionic saw blade for corn stalk cutting," *J. Bionic Eng.*, vol. 10, no. 4, pp. 497–505, Oct. 2013, doi: 10.1016/S1672-6529(13)60242-5.
[5] S. K. Mathanker, T. E. Grift, and A. C. Hansen, "Effect of blade oblique angle and cutting speed on cutting energy for energycane stems," *Biosyst. Eng.*, vol. 133, pp. 64–70, May 2015, doi: 10.1016/j.biosystemseng.2015.03.003.
[6] H. Gan, S. Mathanker, M. A. Momin, B. Kuhns, N. Stoffel, A. Hansen, and T. Grift, "Effects of three cutting blade designs on energy consumption during mowing-conditioning of miscanthus giganteus," *Biomass Bioenergy*, vol. 109, pp. 166–171, Feb. 2018, doi: 10.1016/j.biombioe.2017.12.033.
[7] M. I. A. Halim, Z. N. Musa, S. N. Jaluddin, U. K. A. Karim, M. M. Mahat, M. F. Sufian, and Z. Z. Ariffin, "Investigation of sharpness of knife by onion cutting," *Mater. Today, Proc.*, vol. 16, pp. 2039–2046, Jan. 2019, doi: 10.1016/j.matpr.2019.06.089.
[8] C. Schmidt, H.-H. Westermann, and R. Steinhilper, "An investigation of buzz saw blade cutting forces depending on tool geometry for cutting frozen wood," *Procedia Manuf.*, vol. 33, pp. 778–785, Jan. 2019, doi: 10.1016/j.promfg.2019.04.098.
[9] M. Li, S. Xu, Y. Yang, L. Guo, and J. Tong, "A 3D simulation model of corn stubble cutting using finite element method," *Soil Tillage Res.*, vol. 166, pp. 43–51, Mar. 2017, doi: 10.1016/j.still.2016.10.003.
[10] Y. Meng, J. Wei, J. Wei, H. Chen, and Y. Cui, "An ANSYS/LS-DYNA simulation and experimental study of circular saw blade cutting system of mulberry cutting machine," *Comput. Electron. Agricult.*, vol. 157, pp. 38–48, Feb. 2019, doi: 10.1016/j.compag.2018.12.034.
[11] Y. N. Li, Y. W. Yi, and S. W. Du, "Design and experiment on air blowing header of plot combine harvester for Grain," *Trans. Chin. Soc. Agricult. Machinery*, vol. 48, no. 6, pp. 79–87, Jun. 2017, doi: 10.6041/j.issn.1000-1298.2017.06.010.
[12] J. S. Wang, D. W. Wang, S. Q. Shang, Y. Y. Wang, and J. Kuai, "Development and experiment on 4LZZ-1.0 type plot grain combine," *Trans. Chin. Soc. Agricult. Eng.*, vol. 32, no. 18, pp. 19–22, Mar. 2016, doi: 10.11975/j.issn.1002-6819.2016.18.003.
[13] B. Tang, J. N. Yuan, X. W. Li, B. Zhang, S. Cheng, and K. P. Tian, "Kinamatical analysis and simulation of cutter for hemp mini-type vertical cutting table," *J. Chin. Agricult. Mechanization*, vol. 39, no. 9, pp. 5–8,Aug. 2018, doi: 10.13733/j.jcam.issn.2095-5553.2018.09.001.
[14] W. B. Cao, W. L. Sun, C. Niu, and B. B. and Chen, "Combed safflower picking device based on ANSYS/LS-DYNA," *Trans. Chin. Soc. Agricult. Machinery*, vol. 49, no. 11, pp. 123–131, Jul. 2018, doi: 10.6041/j.issn.1000-1298.2018.11.014.
[15] X. Chen, L. Tang, B. Liu, L. Q. Lv, M. Y. Yang, and J. W. Yang, "Dynamic analysis and simulation of the cutting system of sugarcane harvester," *J. Chin. Agricult. Mechanization*, vol. 39, no. 5, pp. 31–34, May 2018, doi: 10.13733/j.jcam.issn.2095-5553.2018.05.006.
[16] J. H. Ran, S. L. Mu, H. T. Li, Z. H. Guan, Q. Tang, and C. Y. Wu, "Design and test of planet gear driver of reciprocating double-acting cutter for rapeseed combine harvester," *Trans. Chin. Soc. Agricult. Eng.*, vol. 36, no. 9, pp. 17–25, Nov. 2020, doi: 10.11975/j.issn.1002-6819.2020.09.002.
[17] J. Gao, S. Xie, X. Zhang, H. Wang, W. Gao, and H. Zhou, "Study on the 2D optimization simulation of complex five-hole cutting blasting under different lateral pressure coefficients," *Complexity*, vol. 2020, pp. 1–12, Jun. 2020, doi: 10.1155/2020/4639518.
[18] X. Lou, B. Wang, E. Wu, M. Sun, P. Zhou, and Z. Wang, "Theoretical and numerical research on V-Cut parameters and auxiliary cuthole criterion in tunnelling," *Adv. Mater. Sci. Eng.*, vol. 2020, pp. 1–13, Feb. 2020, doi: 10.1155/2020/8568153.
[19] M. Topakci, H. K. Celik, M. Canakci, A. E. W. Rennie, I. Akinci, and D. Karayel, "Deep tillage tool optimization by means of finite element method: Case study for a subsoiler tine," *Food. Agric. Environ*, vol. 8, no. 2, pp. 531–536, Apr. 2010, doi: 10.3168/jds.2010-93-4-1785.
[20] C. Kelln, J. Sharma, and D. Hughes, "A finite element solution scheme for an elastic–viscoplastic soil model," *Comput. Geotechnics*, vol. 35, no. 4, pp. 524–536, Jul. 2008, doi: 10.1016/j.compgeo.2007.10.003.
[21] S. B. Mickovski, A. Stokes, R. van Beek, M. Ghestem, and T. Fourcaud, "Simulation of direct shear tests on rooted and non-rooted soil using finite element analysis," *Ecol. Eng.*, vol. 37, no. 10, pp. 1523–1532, Oct. 2011, doi: 10.1016/j.ecoleng.2011.06.001.
[22] X. P. Li, D. G. Zhou, X. B. Zhou, and Y. and Shao, "Microstructure and fiber size of the castor-oil plant," *J. Zhejiang A&F Univ.*, vol. 26, no. 2, pp. 239–245, Jul. 2009, doi: 10.1016/S1874-8651(10)60073-7.
[23] H. T. Huang, Y. X. Wang, Y. Q. Tang, F. Zhao, and X. F. Kong, "Finite element simulation of sugarcane cutting," *Trans. Chin. Soc. Agricult. Eng.*, vol. 27, no. 2, pp. 161–166, May 2011.
[24] S. Wu and X. H. Wei, "Mechanical interaction between a canopy opener and rice stalks based on the transient dynamic analysis," *Biosyst. Eng.*, vol. 178, pp. 256–263, Feb. 2019, doi: 10.1016/j.biosystemseng.2018.12.004.
[25] F. Kara and A. Takmaz, "Optimization of cryogenic treatment effects on the surface roughness of cutting tools," *Mater. Test.*, vol. 61, no. 11, pp. 1101–1104, Nov. 2019, doi: 10.3139/120.111427.

JUNMING HOU was born in Shenyang, China. He received the M.S. and Ph.D. degrees in mechanical manufacture and automation from the School of Mechanical Engineering and Automation, Northeastern University, China, in 2006 and 2009, respectively. He is currently an Associate Professor with the School of Engineering, Shenyang Agricultural University, China. His research interests include mechanical design, agricultural machinery design, biological system engineering, agricultural product harvesting and processing technology, and fruit production machinery.

JINGBO BAI received the B.S. degree in mechanical engineering and automation from Shenyang Agricultural University, in 2016, where he is currently pursuing the master's degree. His research interests include agricultural machinery design and agricultural information technology.

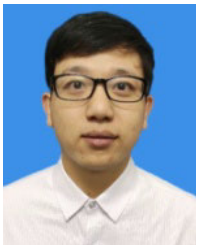

ENCHAO YAO received the B.S. degree in mechanical engineering and automation from Shenyang Agricultural University, in 2017, where he is currently pursuing the master's degree. His research interests include agricultural machinery design, agricultural information technology, and visual inspection of agricultural products.

HONGJIE ZHU received the B.S. degree in mechanical engineering and automation from Shenyang Agricultural University, in 2017, where she is currently pursuing the master's degree. Her research interests include agricultural machinery design and agricultural information technology.